

Integrated In Situ Stress Estimation by Hydraulic Fracturing, Borehole Observations and Numerical Analysis at the EXP-1 Borehole in Pohang, Korea

Hanna Kim¹ · Linmao Xie¹ · Ki-Bok Min^{1,4}  · Seongho Bae² · Ove Stephansson³

Received: 19 March 2017 / Accepted: 17 July 2017 / Published online: 8 August 2017
© Springer-Verlag GmbH Austria 2017

Abstract It is desirable to combine the stress measurement data produced by different methods to obtain a more reliable estimation of in situ stress. We present a regional case study of integrated in situ stress estimation by hydraulic fracturing, observations of borehole breakouts and drilling-induced fractures, and numerical modeling of a 1 km-deep borehole (EXP-1) in Pohang, South Korea. Prior to measuring the stress, World Stress Map (WSM) and modern field data in the Korean Peninsula are used to construct a best estimate stress model in this area. Then, new stress data from hydraulic fracturing and borehole observations is added to determine magnitude and orientation of horizontal stresses. Minimum horizontal principal stress is estimated from the shut-in pressure of the hydraulic fracturing measurement at a depth of about 700 m. The horizontal stress ratios (S_{Hmax}/S_{Hmin}) derived from hydraulic fracturing, borehole breakout, and drilling-induced fractures are 1.4, 1.2, and 1.1–1.4, respectively, and the average orientations of the maximum horizontal stresses derived by field methods are N138°E, N122°E, and N136°E, respectively. The results of hydraulic fracturing and borehole observations are integrated with a result of numerical modeling to produce a final rock stress model. The results of the

integration give in situ stress ratios of 1.3/1.0/0.8 ($S_{Hmax}/S_V/S_{Hmin}$) with an average azimuth of S_{Hmax} in the orientation range of N130°E–N136°E. It is found that the orientation of S_{Hmax} is deviated by more than 40° clockwise compared to directions reported for the WSM in south-eastern Korean peninsula.

Keywords Estimation of in situ stress · Hydraulic fracturing · Borehole breakout · Drilling-induced fractures · Stress integration · Korean Peninsula

1 Introduction

Knowledge of in situ rock stress is critically important in many applications of civil, mining, petroleum, and geothermal engineering, as well as in geology and geophysics (Amadei and Stephansson 1997). Despite significant improvements in the measurement techniques for the estimation of in situ stress, uncertainties are associated with their measurements due to intrinsic rock heterogeneity, size effect, and the difficulty of acquiring reliable data in harsh, underground conditions.

There have been many uncertainties and disagreements concerning the measurement results obtained by various techniques at different rock conditions. Reflecting these uncertainties, the term ‘stress estimation’ has been suggested to replace ‘stress determination’ or ‘stress measurement’ to emphasize the fact that the measurement of stress in rock requires the use of one’s ‘judgment’ or ‘opinion’ (Hudson and Cornet 2003; Fairhurst 2003). Thus, it is desirable to combine the stress measurement data produced by different methods to obtain a more reliable estimation of in situ stress. For example, the measurement of stress during hydraulic fracturing can be supplemented

✉ Ki-Bok Min
kbmin@snu.ac.kr

¹ Department of Energy Systems Engineering, Seoul National University, Seoul, Republic of Korea

² GeoGeny Consultants Group Inc., Seoul, Republic of Korea

³ GFZ German Research Centre for Geosciences, Potsdam, Germany

⁴ Present Address: Department of Energy Systems Engineering, Seoul National University, Seoul, Republic of Korea

by borehole observations or by a core-based method in order to enhance the credibility of the final rock stress model. This integration approach is especially useful when only a limited number of tests from each method is available (Amadei and Stephansson 1997; Zang and Stephansson 2010).

In order to construct a reliable final rock stress model of a site or an area, a set of steps must be followed to gain the required knowledge and data (Stephansson and Zang 2012). Before starting any in situ stress measurement, the geological and morphological characteristics of the area of interest must be considered, and the existing in situ stress measurement data must be collected to establish a stress model that can provide the best estimate. Thereafter, stress measurements are made using borehole methods or core-based methods, and new data are added to construct an integrated stress model. Furthermore, a numerical stress model can be also used to help establish the credibility of the final rock stress model.

There are several case studies that presented an integrated stress model by combining the results of various stress measurements. Vernik and Zoback (1992) combined the results of borehole breakout analyses with the hydraulic fracturing stress measurements at Cajon Pass in the United States. Also, a series of works in the German Continental Deep Drilling Project (KTB) for stress measurement from the natural and induced seismicity, hydraulic fracturing, borehole breakout, drilling-induced fractures, and core-based methods were integrated to determine the state of stress in the deep borehole (Zoback et al. 1993; Brudy et al. 1997). In order to estimate the stress at the Bure experimental test site in northeastern France, Wileveau et al. (2007) reported the results of hydraulic testing on pre-existing fractures (HTPF) and sleeve-fracturing tests, as well as the results of hydraulic fracturing, borehole breakouts, and drilling-induced fractures.

In addition to the direct measurement of stress, numerical modeling can be used as a complementary tool to estimate in situ stress. Numerical analysis was used for the global stress model (Hart 2003) and the interpretation of the overcoring method (Fouial et al. 1998). Rutqvist et al. (2000) presented uncertainties in the maximum principal stress estimated from hydraulic fracturing measurements by coupled hydromechanical modeling. Numerical analysis also can be used to validate the results of existing stress measurements and to help estimate in situ stress as an independent method. Klee et al. (2011) and Shen et al. (2014) conducted boundary element numerical modeling to constrain the magnitude of the in situ stress for the Blanche-1 borehole and the Habanero No. 1 well in South Australia, respectively. Both studies showed that the results of numerical modeling were consistent with actual observations of breakouts at each site, thus numerical analysis can be used as a complementary stress estimation method.

In Korean Peninsula, extensive stress measurements have been conducted mostly using overcoring and hydraulic fracturing and stress models are reported to describe the stress state (Haimson et al. 2003; Choi et al. 2008; Bae et al. 2010; Chang et al. 2010). All of the stress data in deep formation included in WSM is obtained by focal mechanism and there is a dearth of direct measurement data particularly in formation deeper than 500 m (Heidbach et al. 2016). With increasing demand in underground engineering such as CO₂ geological sequestration and Enhanced Geothermal System (EGS), robust characterization of in situ stress in deep formation is necessary.

We present a regional case study of integrated in situ stress model of the EXP-1 borehole in Pohang of Korea using hydraulic fracturing, observation of borehole breakouts and drilling-induced tensile fractures, and numerical modeling. Field observations and numerical analysis were integrated to obtain final rock stress model. This paper starts with best estimate stress model prior to stress measurement campaign, procedure and result of each independent stress measurement with numerical analysis, followed by discussion on final rock stress model.

2 Best Estimate Stress Model

2.1 Geological Data of Pohang

The vertical borehole EXP-1 has a depth of 1002 m and is located in Pohang in the Gyeongsang Basin in southeastern Korea. The Gyeongsang Basin is a Cretaceous sedimentary basin, and it is reported that local scale faults exist extensively throughout the basin. Most of the faults in this area, including Yangsan fault that is about 200 km long, are striking in the NNE direction (Kyung 2003; Chang et al. 2010). Slip analysis and the earthquake focal mechanism have been studied extensively, and most of the studies have shown that the main direction of compression in this area is ENE–WSW (Chang et al. 2010).

The EXP-1 borehole is located about 4 km southeast of the drill site of the Pohang Enhanced Geothermal System (EGS) development project (Fig. 1). With the aim of constructing a 1 MW-scale geothermal power plant (Lee et al. 2011), the EXP-1 borehole was drilled for an initial investigation of the stress field in this area. Currently, two deep boreholes in the depth of 4.35 and 4.217 km are available at the Pohang EGS site, and several scientific investigations, including hydraulic stimulation, are being conducted at the site (Yoon et al. 2015; Kim et al. 2016).

The rock formation at the EXP-1 borehole consists of semi-consolidated mudstone from the surface of the ground to a depth of 650 m, and this is followed by volcanic lapilli tuff. A steel casing was installed from the surface to a depth of 650 m,

Fig. 1 Location of the EXP-1 borehole and the Pohang EGS site in southeastern Korea

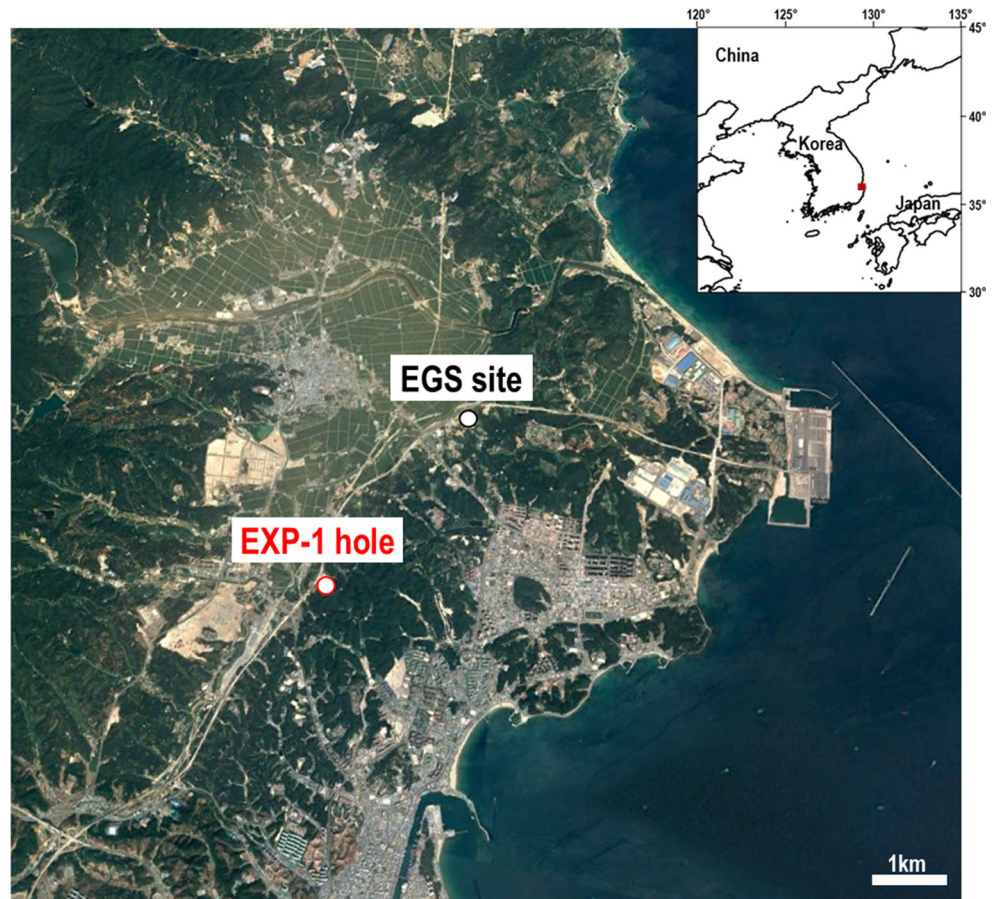


Table 1 Summary of laboratory test result

Properties of rock	Average value
Uniaxial compressive strength (UCS)	80 MPa
Tensile strength	6 MPa
Elastic modulus	50 GPa
Poisson's ratio	0.2
Internal friction angle	34°
Thermal expansion coefficient	$8 \times 10^{-6}/^{\circ}\text{C}$

and cores were extracted from the entire open-hole section between the depths of 650 and 1002 m. Laboratory tests were conducted on the core samples to investigate the rock's properties, including uniaxial compressive strength (UCS), tensile strength, triaxial compressive strength, elastic modulus, and Poisson's ratio (Table 1). In particular, the UCS results of the lapilli tuff exhibited considerable scatter in the depth profile, and they were fitted well by a normal distribution (Fig. 2).

2.2 Available World Stress Map Data near Pohang

It is essential to analyze and refer to stress data from the World Stress Map (WSM) project at an early stage when

deriving a Best Estimate Stress Model (Stephansson and Zang 2012). The 2016 release of the WSM database provided data suggesting that the direction of the maximum compressive stress in southeastern Korea is East-Northeast (E-NE) and that reverse and strike-slip faulting was the dominant faulting regimes (Fig. 3). There are many stress-direction data points in northeastern China and southwestern Japan that can help in estimating the in situ stress around the Korean Peninsula. The direction of S_{Hmax} in northeastern China, which is across the Yellow Sea from west of South Korea, is between E-W and ENE-WSW. In southwestern Japan, the direction of S_{Hmax} is rotated slightly to the south and ranges from E-W to ESE-WNW (Haimson et al. 2003; Heidbach et al. 2016).

3 Stress Measurement Method

3.1 Hydraulic Fracturing Test

Four hydraulic fracturing tests were conducted using a conventional wireline hydrofracturing system in accordance with the International Society for Rock Mechanics' (ISRM's) suggested method for hydraulic fracturing

Fig. 2 **a** UCS data versus depth of lapilli tuff from drill cores of borehole EXP-1; **b** probability density and cumulative density versus UCS of lapilli tuff

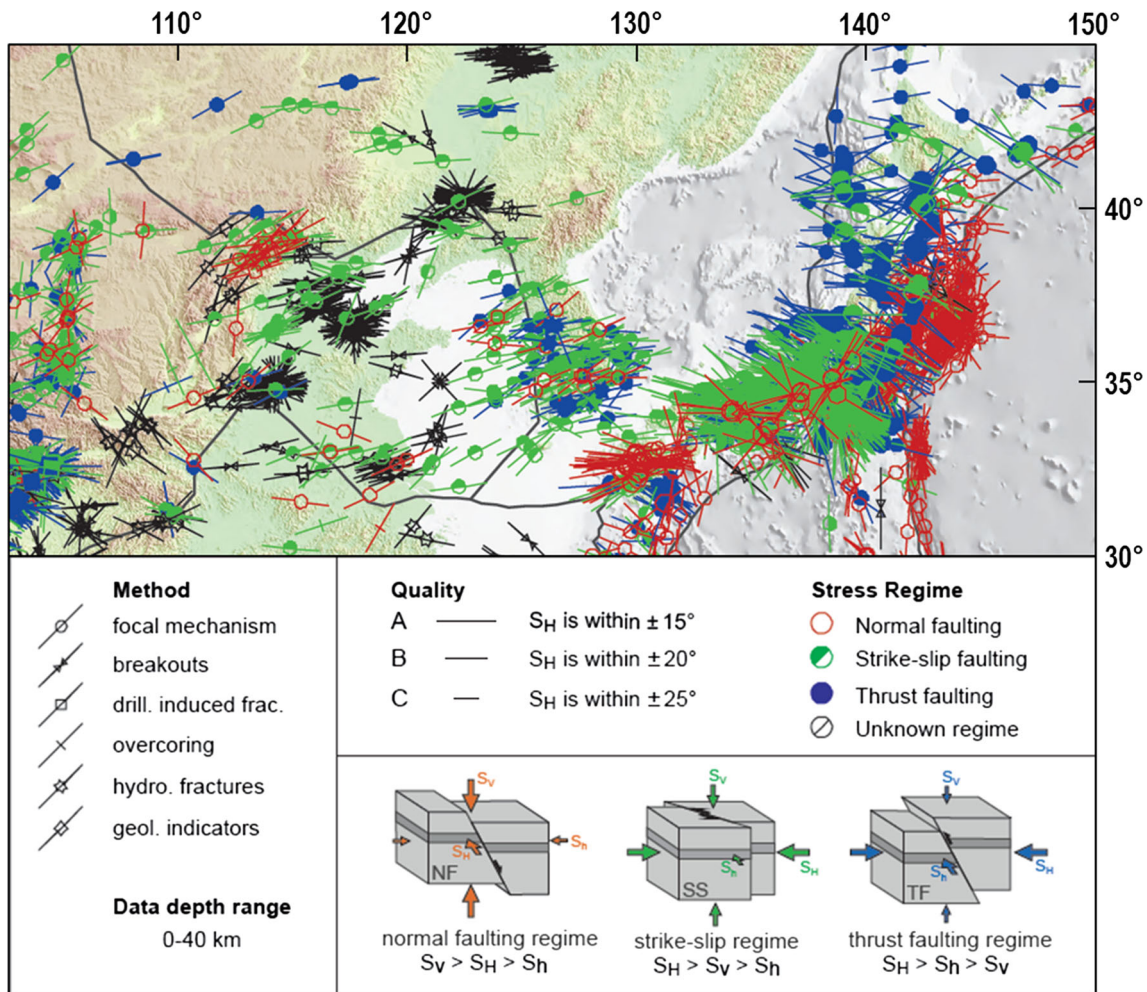
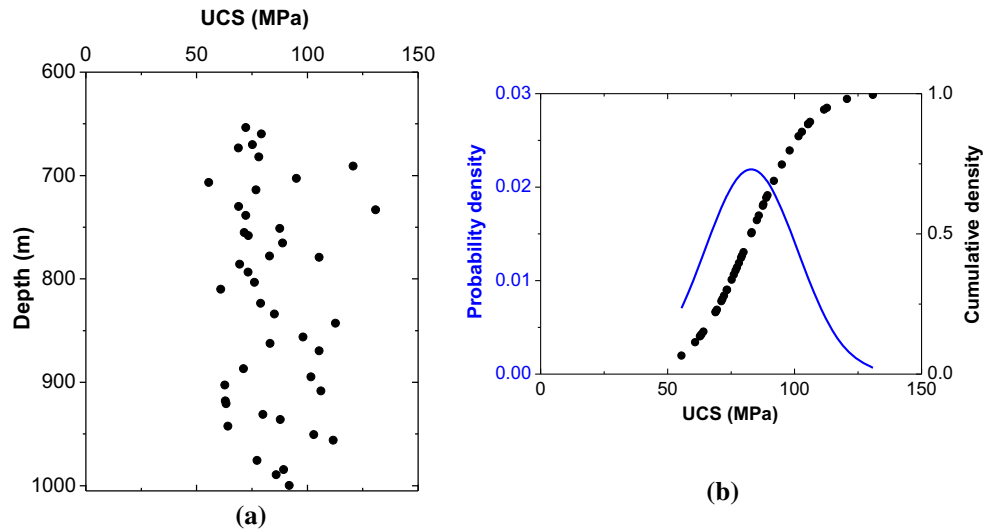


Fig. 3 In situ stress in northeastern Asia from the World Stress Map (Heidbach et al. 2016)

(Haimson and Cornet 2003). Prior to the measurements, test sections without natural fractures were determined from inspection and mapping of the extracted drillcores.

The length of the interval of the straddle-packer was 0.6 m, and the pressure of the test section was set with constant flow rate. During pressurization, the packer pressure was

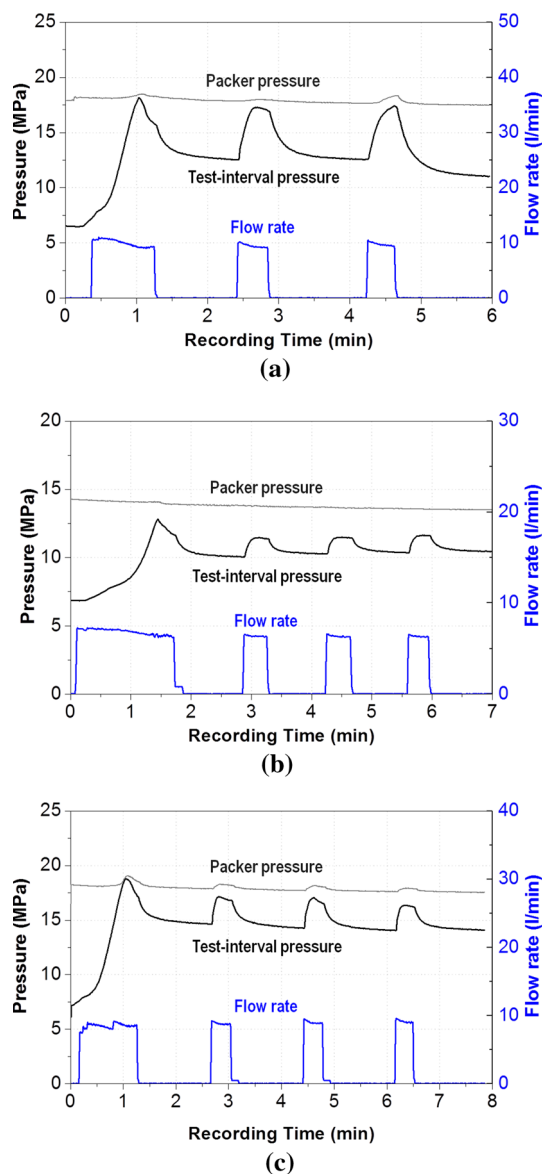


Fig. 4 Test interval and packer pressure and flow rate versus time during hydraulic fracturing in the EXP-1 borehole: **a** depth of 658.5–659.1 m; **b** depth of 685.2–685.8 m; **c** depth of 715.2–715.8 m

maintained somewhat higher than the interval pressure to ensure zero leakage. However, there was a slight decrease in flow rate with time for each pressurization and test interval because of minor leakage (Fig. 4). Three out of four attempts were successful in acquiring the pressure in the packer and test interval section and flow rate data as shown in Fig. 4.

In linear elastic, homogeneous, isotropic, and intact rock, the hydraulic fracture is expected to be vertical and perpendicular to the minimum horizontal stress (S_{hmin}). The acoustic borehole televiwer was used to identify the orientations of the induced fractures after all of the hydraulic fracturing tests were completed. The depth used

in this analysis was calibrated by comparing the pre-existing fractures observed from extracted cores and image logging in order to use a more consistent and accurate depth for analysis. From the televiwer's images in the borehole, vertical hydraulic fractures were observed clearly at two out of three sections. Since the test interval was determined by looking for a section without pre-existing fracture from the extracted core before start of testing, the fractures observed at 685.5–685.8 and 715.2–715.8 m depth section were regarded as hydraulic induced fractures. The images of induced vertical hydrofractures were not in the ideal form of two straight lines 180° apart, and the traces showed discontinuous, en echelon, and off-center fractures (Fig. 5). Circular statistics were applied to determine the orientation of the fractures (Lee and Haimson 1989), which is recommended to remove the subjectivity and gives the uniformity and confidence in estimation of fracture orientation (Amadei and Stephansson 1997). The mean strike of the fracture was determined to be $N138^\circ E (\pm 3^\circ)$ (Table 2).

The shut-in pressure (P_s) corresponds to the minimum horizontal stress (S_{hmin}) (Haimson and Cornet 2003). It is a common practice to determine the P_s in the pressure–time curve graphically when the initial decrease of the pressure is clearly observed after the pumping has been shut off. However, if the pressure decrease is gradual and the determination of P_s is not distinct, Lee and Haimson (1989) suggested three statistical analyses to determine the shut-in pressure, i.e., (1) the exponential pressure-decay method, (2) the bilinear pressure-decay-rate method, and (3) the pressure–flow rate method. Methods (1) and (2) were used to in this study determine the P_s , and the results were in good agreement. The breakdown pressure (P_b) was obtained graphically from the maximum pressure after the injection of water in the first pressure cycle, and the pore pressure (P_o) was assumed to be the same as the hydrostatic pressure. The results of the hydraulic fracturing tests are shown in Table 2. The P_s does not increase linearly with depth, but it is not uncommon to observe the less P_s at the deeper depths, which seems to be related to natural uncertainty (Amadei and Stephansson 1997) such as the heterogeneity of the strength as shown in Fig. 2a.

If we assume that the rock is impermeable (Lee and Haimson 1989; Haimson and Cornet 2003), the maximum horizontal stress (S_{Hmax}) can be calculated using the Hubbert–Willis–Scheidegger criterion (Eq. (1)) (Hubbert and Willis 1957; Amadei and Stephansson 1997; Zang and Stephansson 2010):

$$S_{Hmax} = 3S_{hmin} - P_b - P_o + T \quad (1)$$

where P_b is the breakdown pressure, P_o is the pore pressure, and T is the tensile strength of the rock, which is 6 MPa in this study (Table 1). The tensile strength was

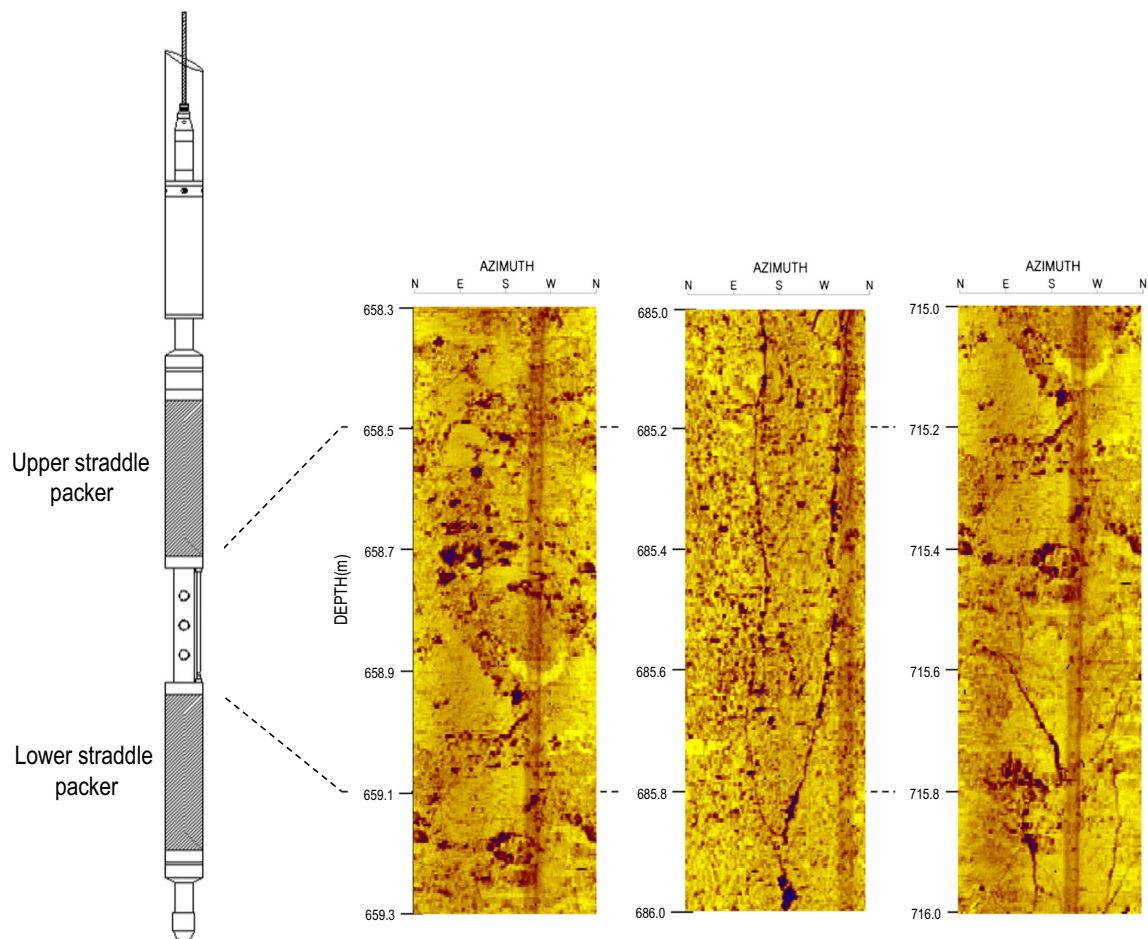


Fig. 5 Acoustic borehole televiwer images of induced hydraulic fractures at depths of 658.3–659.3, 685–686, and 715–716 m

Table 2 Results of the hydraulic fracturing measurements in borehole EXP-1

Depth (m)	Breakdown pressure (P_b), MPa	Shut-in pressure (P_s), MPa	Pore pressure (P_o), MPa	Direction of S_{Hmax}
658.5–659.1	18.2	13.9	6.6	–
685.2–685.8	12.8	10.8	6.8	N135°E
703.1–703.7	Failed			
715.2–715.8	18.8	14.9	7.2	N141°E
Average	16.6	13.2	6.9	N138°E

determined from the Brazilian test by assuming that there were no significant differences in the tensile strengths obtained from the Brazilian test and the hollow-cylinder test. The influence of the thermal stress caused by the thermal disturbance due to the temperature difference between the injection fluid and the rock was considered to be negligible. Compared to the drilling operation, the hydraulic fracturing has relatively small contact area between the injection fluid and rock (0.6 m in this study) and short contact time (several minutes in this study).

As a result, the average S_{Hmax} was calculated to be 22.4 MPa from Eq. (1), and the horizontal stress ratio (S_{Hmax}/S_{Hmin}) was 1.7.

3.2 Borehole Breakouts

Borehole breakout occurs at the azimuth of the minimum horizontal stress, and it is used as a reliable indicator to estimate the orientations of the principal horizontal stresses (Bell and Gough 1979; Plumb and Hickman 1985; Tingay et al. 2008; Stephansson and Zang 2012). In addition,

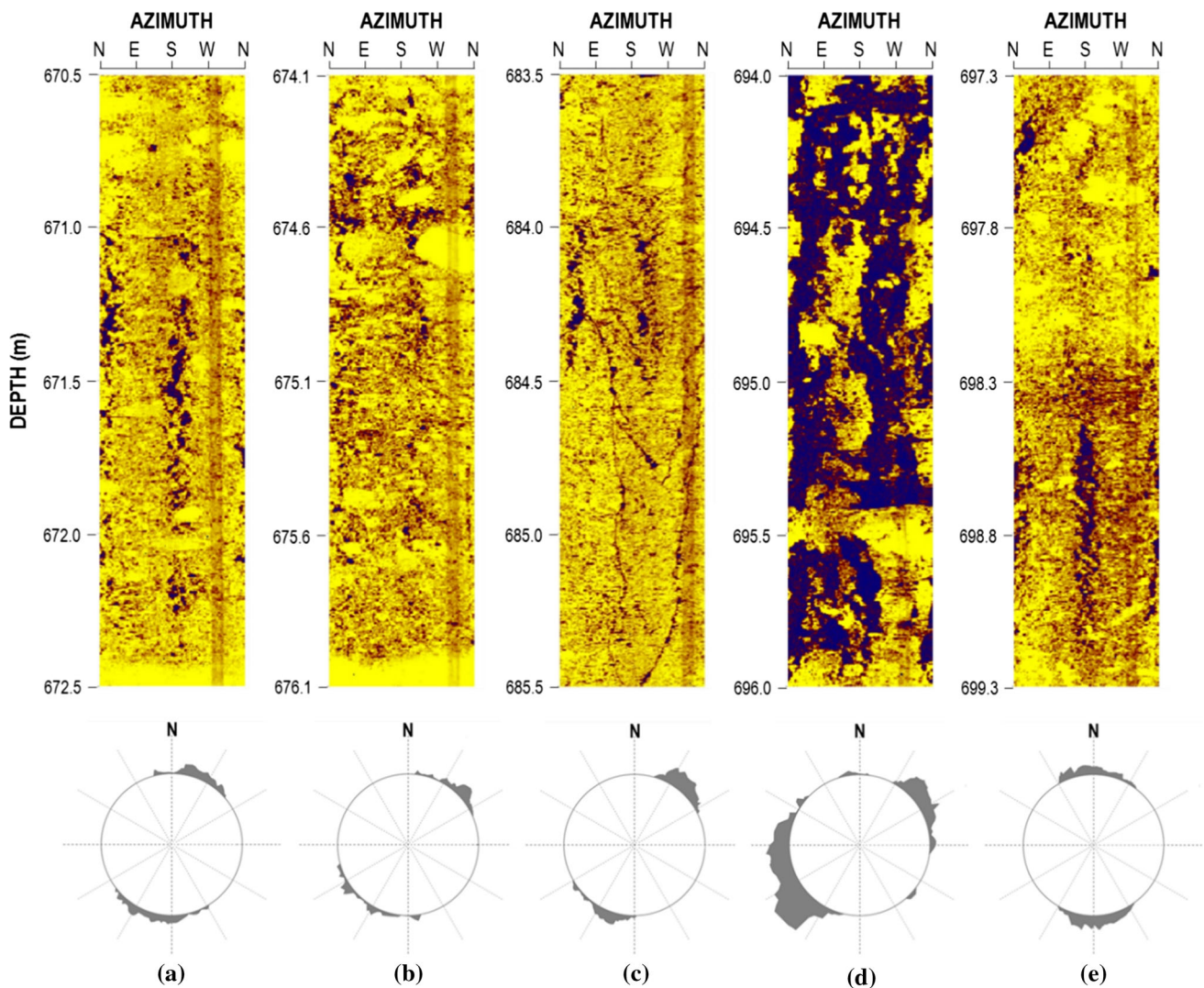


Fig. 6 Acoustic borehole televiwer images of borehole breakouts in selected sections of borehole EXP-1 (*above*) and corresponding horizontal section views (*below*)

because the geometry of breakouts depends on the type of rock and the magnitude of the in situ stress, there have been many attempts to use the geometry of the breakouts to determine the magnitude of the in situ stress (Zoback et al. 1985; Barton et al. 1988; Vernik and Zoback 1992; Brudy et al. 1997; Zoback et al. 2003; Shen et al. 2014). It was emphasized that analyses of borehole breakout that consider both length and width should use the shape that is observed immediately after the occurrence of borehole breakouts (Zoback et al. 1985). However, in this study, image logging was conducted several dozen days after drilling, and, therefore, only the width of the breakout was considered to estimate the magnitude of S_{Hmax} (Barton et al. 1988). The premise of this analysis was that the breakouts form in the area around a wellbore where the local stress concentration exceeds the strength of the rock; the width of the breakout remains stable, but the depth of

the breakout increases with time. Numerous sites, including Fenton Hill and Cajon Pass in the United States and KTB in Germany, have shown that the width of breakout can be used as an independent observation to estimate the in situ stress in combination with the data from hydraulic fracturing measurements and the analysis of the focal mechanism (Barton et al. 1988; Vernik and Zoback 1992; Brudy et al. 1997).

The logs obtained by the borehole televiwer at EXP-1 borehole showed that several breakouts occurred in the borehole wall at depths between 670 and 700 m (Fig. 6). The breakout images were ranked as C-quality according to the WSM guideline, because five distinct breakout zones were observed and the combined breakout lengths were longer than 20 m in a single well (Tingay et al. 2008). The orientations of the breakouts were estimated using circular statistics and the breakouts had nearly consistent azimuths,

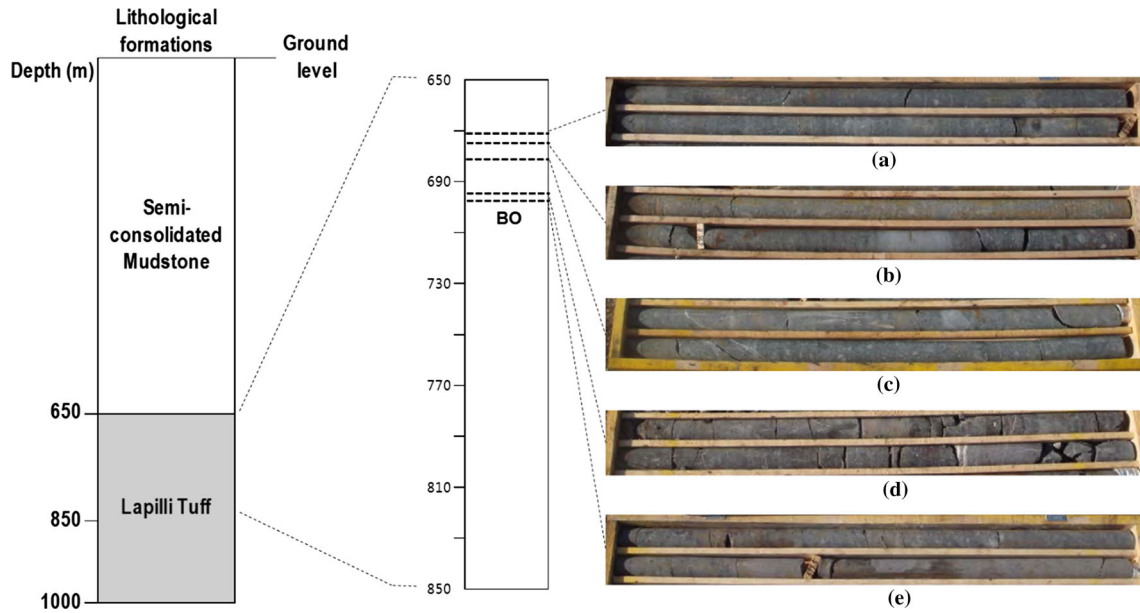


Fig. 7 Pictures of core samples of lapilli tuff extracted from depths at which borehole breakouts occurred

with an average value of $N26^{\circ}E \pm 13^{\circ}$. The only exception was at a depth of about 699 m, where breakouts occurred in the N-S direction.

The sparsely observed borehole breakouts that had large variations in their shapes were likely caused by the effect of the variable strength of the heterogeneous rock rather than by any major changes in the in situ stress condition. The widest and deepest breakout was observed at a depth of about 695 m, which is explained by more fractures identified from rock core samples (Fig. 7d).

Assuming that a borehole breakout occurs when the tangential stress around the wall of the borehole caused by the given in situ stress condition exceeds the critical strength, the maximum principal stress can be obtained from the following equation (Barton et al. 1988; Vernik and Zoback 1992; Brudy et al. 1997):

$$S_{Hmax} = \frac{(P_0 + C_{eff}) - S_{hmin}(1 + 2 \cos 2\theta_b)}{1 - 2 \cos 2\theta_b}, \quad (2)$$

where θ_b is the angle of breakout initiation with respect to S_{Hmax} ; Φ_b is the half width of the breakout ($\Phi_b = \pi/2 - \theta_b$) (Fig. 8); P_0 is the pore pressure; and C_{eff} is the effective strength of the rock when the breakout occurs. Temperature effect is often included in the borehole breakout analysis since the cold wellbore cooling due to drilling fluid exerts a tensile thermal stress on the tangential direction around the borehole (Zoback 2007). However, in this analysis, we did not consider temperature effect because the temperature was believed to be recovered to the initial one since the observation of borehole breakout by televiewer logging was made dozens of days after the drilling. As temperature recovery

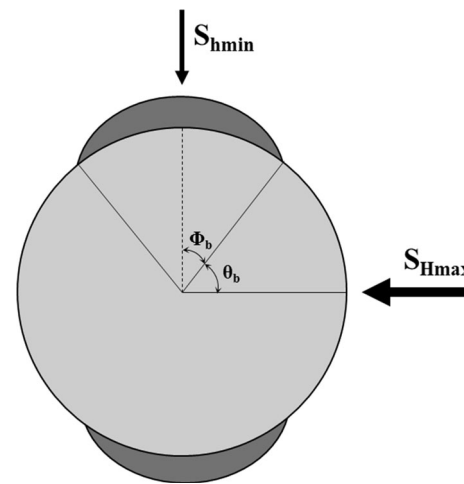


Fig. 8 Schematic of borehole breakouts in the direction of S_{hmin} showing the angles Φ_b and θ_b

contributes to the larger compressive tangential stress, it is more likely that breakout occurred when the temperature recovered. This is in contrast to the drilling-induced fractures explained in the next section where cold drilling fluid directly contributes to the generation of tensile fractures and the consideration of cold temperature is essential.

The stress condition at the borehole wall is polyaxial (or true triaxial) state; therefore, it is reasonable to use the polyaxial criteria to predict the failure of wellbore. We used the modified Wiebols and Cook criterion (Eq. (3)) to determine the effective strength (C_{eff}) when the breakout occurs. And the parameters making up the criterion can be constrained by rock strengths under

uniaxial and triaxial conditions; thus, the UCS and internal friction angle (μ_i) determined from uniaxial and triaxial tests are used to determine the effective strength (Zhou 1994; Colmenares and Zoback 2002; Jaeger et al. 2009).

$$J_2^{1/2} - A - BJ_1 - CJ_1^2 = 0$$

where

$$J_1 = \frac{\sigma_1 + \sigma_2 + \sigma_3}{3}$$

$$J_2 = \frac{(\sigma_1 - \sigma_2)^2 + (\sigma_2 - \sigma_3)^2 + (\sigma_3 - \sigma_1)^2}{6}$$

$$C = \frac{\sqrt{27}}{(2C_1 + (q - 1)\sigma_3 - UCS) \cdot \left(\frac{C_1 + (q - 1)\sigma_3 - UCS}{2C_1 + (2q + 1)\sigma_3 - UCS} - \frac{q - 1}{q + 2} \right)}$$

$$C_1 = (1 + 0.6\mu_i) \cdot UCS$$

$$q = \left(\sqrt{\mu_i^2 + 1} + \mu_i \right)^2$$

$$B = \frac{\sqrt{3}(q - 1)}{q + 2} - \frac{C}{3} (2 \cdot UCS + (q + 2)\sigma_3)$$

$$A = \frac{UCS}{\sqrt{3}} - \frac{UCS}{3} \cdot B - \left(\frac{UCS}{3} \right)^2 \cdot C$$

The probability density function for C_{eff} was generated by Monte Carlo simulation based on normal distribution of UCS. Then, the C_{eff} function was combined with different combination sets of in situ stress, S_{Hmax} , and S_{hmin} to estimate the breakout width, $2\Phi_b$. Mean prediction errors (MPEs), as defined in Eq. (3), were calculated to determine the best set of combined in situ stresses:

$$MPE = \frac{1}{N} \sum_{i=1}^N \left| \frac{\Phi_{bi}^o - \Phi_{bi}^p}{\Phi_{bi}^o} \right|, \tag{4}$$

where Φ_{bi}^o is the angle observed in the field, Φ_{bi}^p is the theoretically predicted angle, and N is the number of prediction points within the borehole section showing breakouts. As a result, the horizontal in situ stress ratio was determined to be optimal when the value of MPE was a minimum.

Figure 9 shows the probability function of the breakout width ($2\Phi_b$) for different horizontal stress ratios, i.e., S_{Hmax}/S_{hmin} , of 1.6, 1.65, and 1.7. The calculated MPEs of $2\Phi_b$ for the three ratios were 74, 64, and 77%, respectively, which shows that horizontal stress ratio of 1.65 was the most appropriate value of minimum error. Although the graph does not give a perfect fit, the function we used had a reasonable fit with the field observations considering the heterogeneity of the rock and a few outlier values of $2\Phi_b$ around 60° and 120°.

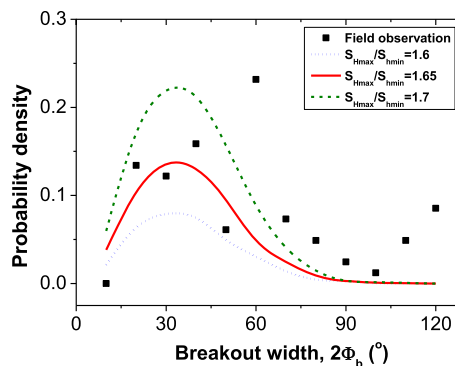


Fig. 9 Probability density versus breakout width and field observation of breakouts for the section of the EXP-1 borehole from 670 to 700 m: The optimum probability density function of breakout width ($2\Phi_b$) was obtained when the horizontal stress ratio (S_{Hmax}/S_{hmin}) was 1.65 (solid line)

3.3 Drilling-Induced Fractures

Another important indicator that can be used to estimate the in situ stress is drilling-induced fractures (DIFs). DIFs form when the stress concentration at the wall of the borehole exceeds the tensile strength of the rock, and they typically develop with sharply narrow fracture features and are parallel to the S_{Hmax} direction (Tingay et al. 2008).

In the EXP-1 borehole, DIFs were recognized in the borehole televiewer images at depths in the range of 775–810 m, which was somewhat deeper than where breakouts occur. Six distinct zones of the DIFs were observed, and the combined length was around 20 m, and, therefore, the quality of the data was ranked as a C-quality based on the quality ranking criteria of WSM (Tingay et al. 2008). The average orientation of the combined DIFs, which was calculated by circular statistics, was $N136^\circ E \pm 4^\circ$ (Fig. 10). In addition to the in situ stress state, the pressure and temperature of the drilling fluid (mud) affect the stresses that are concentrated around the borehole (Brudy and Zoback 1999; Zoback 2007). When the mud is cooler than the formation’s rock, the thermally induced stresses cause more concentrated tensile stress, and DIFs are formed. The condition that initiates the DIFs can be derived from Eq. (1) by considering the additional thermal stress (Brudy and Zoback 1999; Zoback 2007):

$$\sigma^{\Delta T} = - \frac{\alpha \cdot E \cdot \Delta T}{1 - \nu}, \tag{4}$$

where α is the thermal expansion coefficient, E is Young’s modulus, ν is Poisson’s ratio, and ΔT is the difference between the temperature of the mud and the temperature of the rock, which was assumed to be 10 °C for the conservative analysis of DIFs.

Brudy et al. (1997) reported that the tensile strength of the rock does not have to be considered for the analysis of

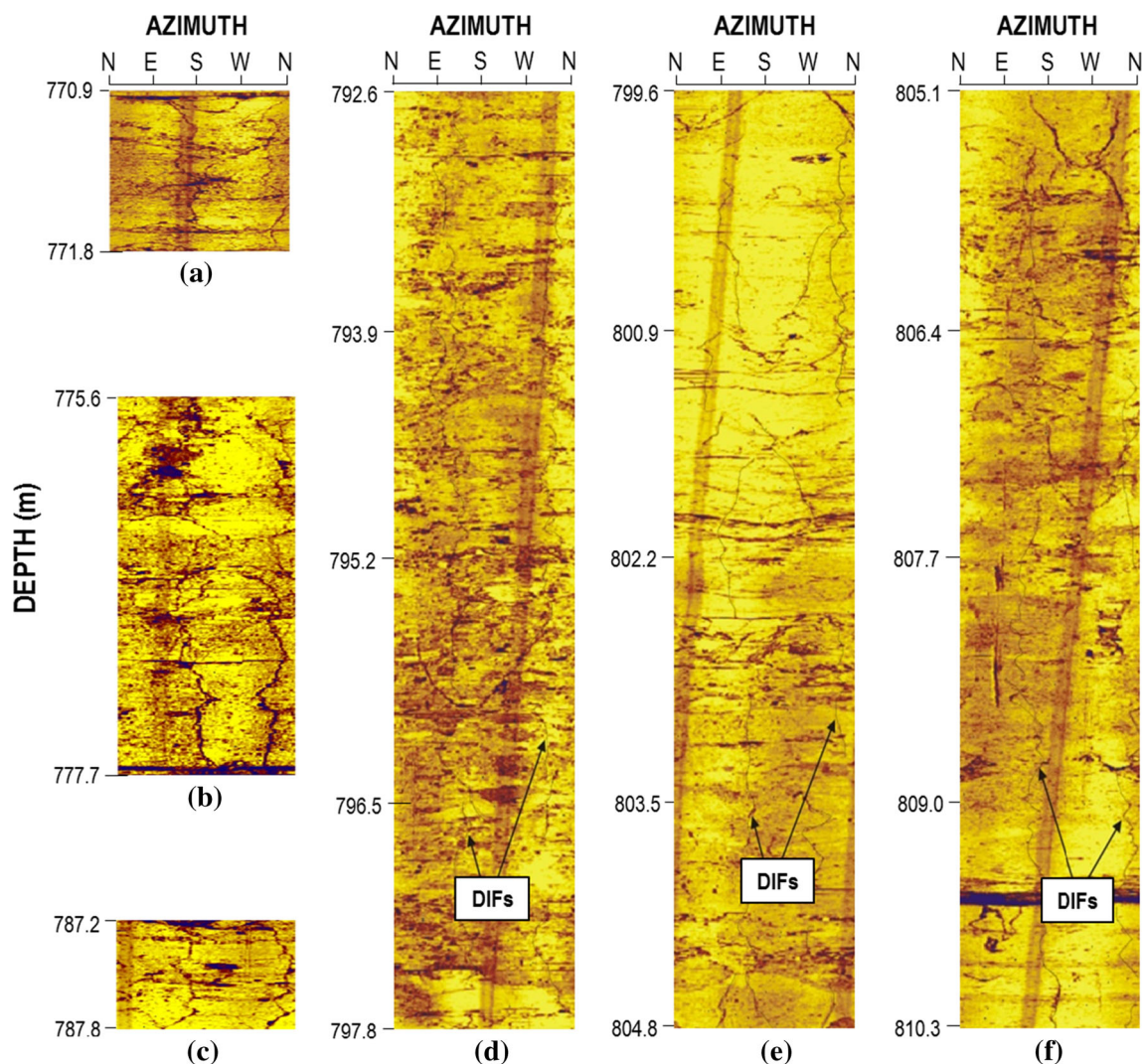


Fig. 10 Acoustic borehole televiewer images of drilling-induced fractures (DIFs) in selected sections of borehole EXP-1: Based on circular statistics, the average orientation of the DIFs for the selected intervals was $N136^{\circ}E \pm 4^{\circ}$

DIFs, because DIFs likely develop from sections in the borehole wall that have small flaws. However, we did not consider the effect of natural fractures on the initiation of DIFs because no natural fractures were observed in the core samples extracted at the depth where DIFs developed.

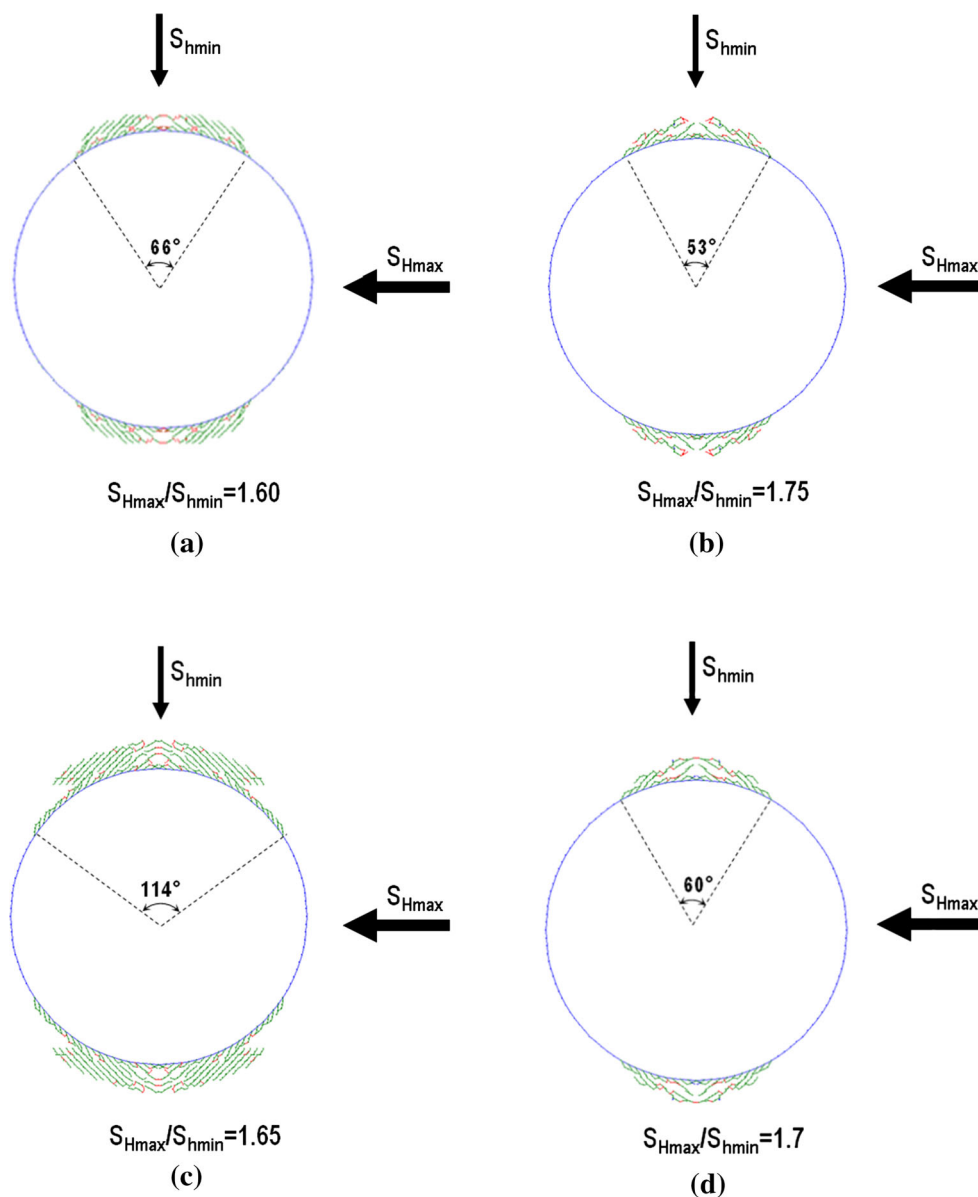
We considered that the DIFs occur in normal drilling conditions with mud. Wiprut and Zoback (2000) showed no correlation between DIFs and special conditions where large change in pressure takes place, such as tripping bit or reaming hole. The maximum mud pressure was assumed to be twice the hydrostatic pressure and used as the static mud pressure in this analysis, since the maximum equivalent circulating density was not available. If we use the maximum mud pressure, the conservative estimation is possible, including the conditions in which the fractures occur at the mud pressure lower than the value we used. This method was used in KTB scientific drilling project (Brudy et al.

1997) and Visund oil field in the northern North Sea (Wiprut and Zoback 2000) as a way to constrain the reliable bound of S_{Hmax} . In order to provide the most conservative estimate of stress as a lower bound, it was assumed that the fractures were developed by the thermal stress from the circulating drilling fluid, whereas, to estimate the upper bound, we assumed that the mud pressure and the in situ stresses were sufficient to cause the DIFs. The maximum horizontal stress, S_{Hmax} , were calculated to be in the range of 20.9 (lower bound) to 27.6 MPa (upper bound), and the stress ratio, S_{Hmax}/S_V , varied from 1.1 to 1.4.

3.4 Numerical Modeling

Numerical modeling is recommended as a complementary tool to predict and validate the in situ stress for the

Fig. 11 Results of numerical modeling with FRACOD. Borehole breakout geometry is presented for a given ratio of S_{Hmax}/S_{Hmin} that gives the best similarity with the observed borehole breakout geometry at a given depth section in borehole EXP-1: **a** depth of 671–676 m; **b** depth of 684–685 m; **c** depth of 694–696 m; **d** depth of 698–699 m



development of the final rock stress model (Zang and Stephansson 2010). In this study, we used FRacture propagation CODE (FRACOD) to conduct the numerical modeling required to simulate the initiation and propagation of borehole breakouts. FRACOD is a boundary element method program that uses the principles of fracture mechanics to predict the explicit fracturing process in rocks (Shen et al. 2014; Shen 2014). Four distinct cross sections were selected at different depths in the EXP-1 borehole for modeling with numerical modeling and to compare the results with the breakout observations. The mechanical properties used in the numerical analysis were based on the laboratory data in Table 1. Since the laboratory test for the fracture toughness was not performed, it was assumed that Mode I and II toughness were 1 and 2 MPa m^{1/2},

respectively, based on measurement in similar rock types (Backers and Stephansson 2015). The minimum horizontal stress, S_{hmin} , was obtained from measurements of hydraulic fracturing, and numerical analysis was conducted for range of the horizontal stress ratios (S_{Hmax}/S_{hmin}). The resulting dimensions of the breakout from numerical modeling were measured to determine the horizontal stress ratio that produced results that were most similar to the actual observations from the televiewer in the borehole.

Figure 11 shows the results of numerical modeling at four different depths in borehole EXP-1. The breakout angles, which are defined as the azimuth angle of the breakout at the wall of the borehole, were almost consistent with the observations from the televiewer. There were differences between the numerical results and the actual

Table 3 Summary of stress ratios and orientation from each of the stress measurement methods and integrated stress determination

	S_{hmin}/S_V	S_{Hmax}/S_V	Average azimuth of S_{Hmax}
Stress measurement method			
Hydraulic fracturing test (HF)	0.8	1.4	N138°E
Borehole breakouts (breakouts)	0.8 (from HF)	1.2	N122°E
Drilling-induced fractures (DIFs)	0.8 (from HF)	1.1–1.4	N136°E
Numerical modeling (modeling)	0.8 (from HF)	1.3–1.4	N122°E (from breakouts)
Integrated stress determination (ISD)	0.8	1.3	N130°E–N136°E

The values in parentheses are the values used for the calculation of ISD

observations at the relatively deeper breakout sections (Fig. 11b, c). There are two possible reasons for this, i.e., (1) the time between drilling and logging was not considered in simulating the breakouts, and, once the breakouts begin to occur, the stress concentration in the vicinity of the breakage zone changes with time and (2) the selection of the mechanical parameters for modeling is the another reason; the results from numerical modeling simulations are sensitive to the values that are selected for the strength and deformability of the intact rock and the fractures that are generated. The UCS at each depth of in the simulation changed for each analysis of the breakouts, while the internal friction angle and fracture toughness were set as constant values for all of the simulations.

4 Determination of the Integrated Stress and the Final Rock Stress Model

After the best estimate stress model was established and new data were collected and analyzed from the different stress measurements, the determination of the integrated stress is the last step in constructing the final rock stress model. In order to integrate the data from the hydraulic fracturing measurements, borehole observations, and the numerical analysis of borehole breakouts, the weighted average method was used for the integration. We transformed each stress tensor to a common set of reference axes, averaged the six components separately, and then calculated the principal stresses of the resultant tensor (Hudson and Cooling 1988; Walker et al. 1990). The weighting factors for the different methods of estimating stress are not necessarily the same, and they must be corrected for specific biases, which may come from the number of tests or the nature and quality of the measurements (Cornet 2015). The hydraulic fracturing data were given more weight than data from borehole observation and numerical analysis, because hydraulic fracturing is a direct method of measuring stress. The mean value of the average azimuth of S_{Hmax} was N130°E, which is equal to the minimum value from applying Integrated Stress Determination (ISD) (Table 3).

Figure 12 shows the orientation and magnitude of stress versus depth from each of the methods and the results of the integrated stress determination down to a depth of 1 km. The vertical stress, S_V , was assumed to be the weight of the overburden for a measured rock density along the entire depth. The minimum horizontal stress, S_{hmin} , was obtained from hydraulic fracturing, and the stress ratio, S_{hmin}/S_V , was 0.8. The stress ratios of S_{Hmax}/S_V derived from hydraulic fracturing, borehole breakout, drilling-induced fractures, and numerical modeling were 1.4, 1.2, 1.1–1.4, and 1.3–1.4, respectively. The orientations of the S_{Hmax} from each method except numerical modeling were N138°E, N122°E, and N136°E. Weighting factors from 0.25 to 0.8 were used for the hydraulic fracturing data, and weighting factors for the other methods were set from 0.07 to 0.25. The azimuth of S_{Hmax} varied from 130°E to 136°E for the given weighting values. The integrated stress magnitude ratios of 1.3/1.0/0.8 ($S_{Hmax}/S_V/S_{hmin}$) resulted in a strike-slip stress regime.

Synn et al. (2013) proposed a relationship between stress ratio and depths down to 700 m that was based on stress measurement data, a geological paleo-stress analysis, and earthquake focal mechanism solutions. Figure 13 shows a compilation of minimum stress ratio ($K_h = S_{hmin}/S_V$) and maximum stress ratio ($K_H = S_{Hmax}/S_V$) with the depth for the Korean peninsula presented in Synn et al. (2013) and stress ratios from the integrated stress estimates from this study for depths in the range of 650–1000 m in borehole EXP-1. Two envelopes suggested by Synn et al. (2013) provide the upper and lower bounds of the data, and the stress ratios decrease with depth. The upper bounds of K_h and K_H at the depth of 1000 m approach 1 and 1.5, respectively, which indicates that a strike-slip stress regime is dominant at depths around 1 km in Korea. The results of the integrated in situ stress model are shown by the dotted line in Fig. 13, and the lines are close to the upper bounds of K_h and K_H .

The stress orientation varies extensively in the Korean Peninsula, but, overall, the predominant direction of S_{Hmax} is ENE–WSW at greater depths (Chang et al. 2010; Synn et al. 2013). This is in general agreement with the E–W trend of the data in the World Stress Map (Heidbach et al. 2016). The integrated S_{Hmax} azimuth of ISD in this

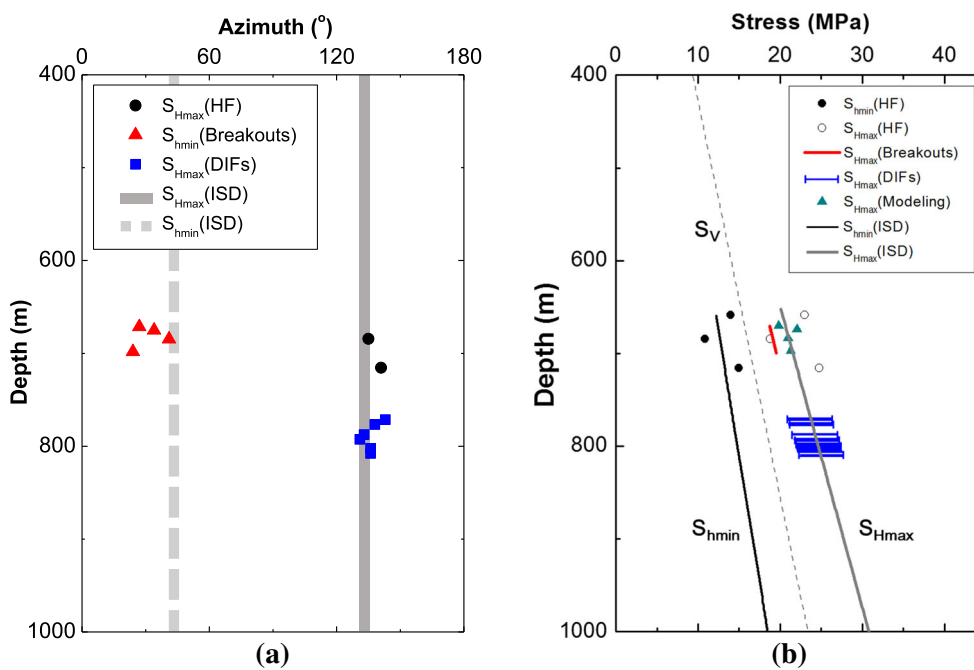
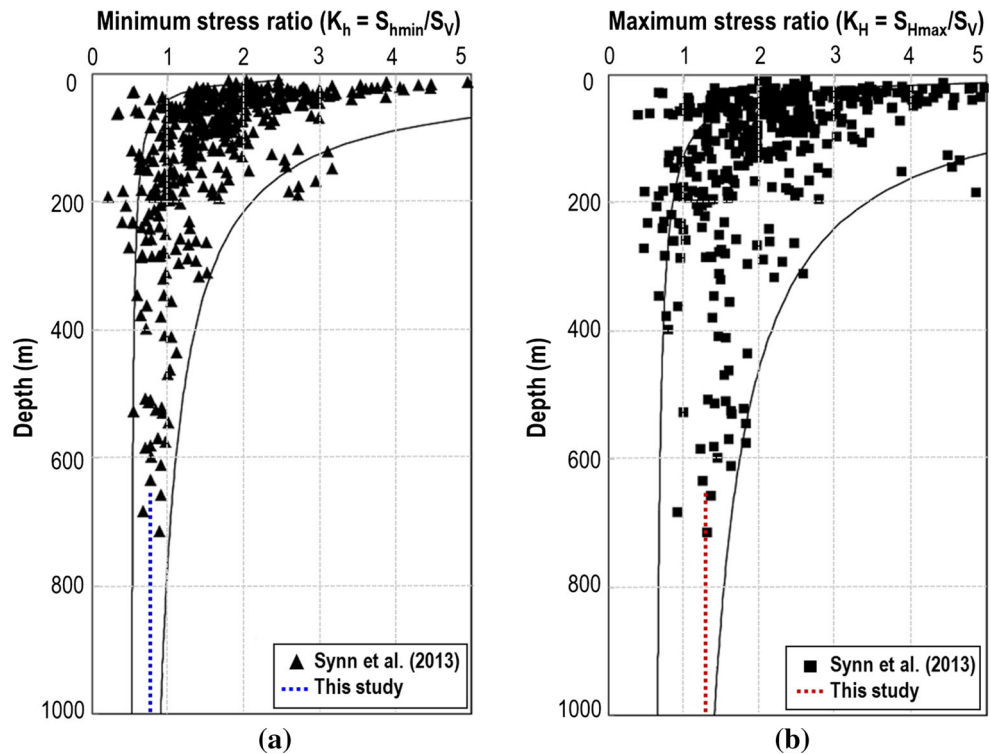


Fig. 12 Orientation and magnitude of stress versus depth from all of the methods used and the results of integrated stress determination (ISD): **a** orientation of horizontal stress with depth; **b** magnitude of

rock stress derived from hydraulic fracturing measurements (HF), analysis of borehole breakout (breakout), drilling-induced fractures (DIFs), and numerical modeling (modeling)

Fig. 13 Compilation of minimum and maximum stress ratios versus depth in the Korean peninsula modified based on Synn et al. (2013) and stress ratios from the integrated stress analyses conducted in this study (dotted line)



study was between N130°E and N136°E, and it deviated more than 40° clockwise compared to E–W and ENE–WSW directions. It should be noted that WSM data in Korea are mostly based on the earthquake focal

mechanism solution, and their depth is greater than 5 km. In addition, the orientation of S_{Hmax} in the southeastern part of Korean peninsula where Pohang is located is heterogeneous even in focal mechanism results, which is

mainly attributed to the effect of regional-scale faults (Chang et al., 2010).

Another estimate of the stress in the Pohang offshore site located about 8 km southeast of the EXP-1 borehole showed that the direction of $S_{H_{\max}}$ from the breakout observation down to 700 mbsf (meter below seafloor) is NW–SE direction and that the stress state from the leak-off test (Chang et al. 2016) is in favor of strike-slip faulting. The results of the offshore study and our study were in agreement concerning the ESE–WNW direction of $S_{H_{\max}}$ of the strike-slip stress regime in southwestern Japan. This regime belongs to the eastern edge of the Eurasian (or Amurian) plate, and, according to data in the WSM compilation, the global stress pattern rotates in a clockwise direction toward the east of the plate (Fig. 3).

5 Conclusions

In this study, a final rock stress model at the EXP-1 borehole which is 4 km away from the ongoing EGS project in Pohang, was established from an integration of the results from hydraulic fracturing and borehole observations. Numerical modeling with boundary element method was also used to constrain the magnitude of the estimates of the in situ stress.

The measurement of the shut-in pressure from hydraulic fracturing was considered to be a reliable estimate of the minimum horizontal principal stress. The maximum stress ratios ($S_{H_{\max}}/S_v$) derived from hydraulic fracturing, borehole breakout, drilling-induced fractures, and numerical modeling were 1.4, 1.2, 1.1–1.4, and 1.3–1.4, respectively. The average orientations of the maximum horizontal stress from each method, with the exception of numerical modeling, were N138°E, N122°E, and N136°E, respectively. The results of the independent stress estimation methods showed that the EXP-1 hole is located in a strike-slip stress regime. An integrated stress was conducted using weighting factors for the magnitude and orientation of $S_{H_{\max}}$, which resulted in situ stress ratios of 1.3/1/0.8 ($S_{H_{\max}}/S_v/S_{H_{\min}}$) with the azimuth of $S_{H_{\max}}$ being N130°E–N136°E for depths between 650 and 1000 m.

The resulting in situ stress model was compared with published stress data for Korean Peninsula. There was good agreement between the published stress models and our results, except that the azimuth of $S_{H_{\max}}$ deviated by more than 40° clockwise compared to the E–W and ENE–WSW directions reported for the WSM and in previous studies.

This regional case study presented an integrated in situ stress model up to a depth of 1 km at the EXP-1 borehole. The stress model can contribute to the description of the in situ stress condition down to a depth of 1 km in the Pohang area. To provide in situ stress model for geothermal

reservoir deeper than 4 km for the ongoing EGS project in Pohang, additional integrated in situ stress estimation is necessary using extracted core samples, indicators in boreholes and hydraulic stimulations results.

Acknowledgements This work was supported by the New and Renewable Energy Technology Development Program of the Korea Institute of Energy Technology Evaluation and Planning (KETEP) through a grant funded by the Korean Government's Ministry of Trade, Industry & Energy (No. 20123010110010). The authors are thankful to The Research Institute of Energy and Resources, Seoul National University.

References

- Amadei B, Stephansson O (1997) Rock stress and its measurement. Springer, Dordrecht
- Backers T, Stephansson O (2015) ISRM suggested method for the determination of mode II fracture toughness. In: Ulusay R (ed) The ISRM suggested methods for rock characterization, testing and monitoring: 2007–2014. Springer International Publishing, Cham, pp 45–56
- Bae S, Kim J, Jeon S, Lee C (2010) Evaluation on the overall characteristics of in situ stress state by hydraulic fracturing test in Korea. In: ISRM international symposium-6th Asian rock mechanics symposium. International Society for Rock Mechanics, New Delhi, India, ARMS6-2010-018, pp 1–9
- Barton CA, Zoback MD, Burns KL (1988) In-situ stress orientation and magnitude at the Fenton Geothermal Site, New Mexico, determined from wellbore breakouts. *Geophys Res Lett* 15:467–470
- Bell JS, Gough DI (1979) Northeast–southwest compressive stress in Alberta evidence from oil wells. *Earth Planet Sci Lett* 45(2):475–482
- Brudy M, Zoback M (1999) Drilling-induced tensile wall-fractures: implications for determination of in situ stress orientation and magnitude. *Int J Rock Mech Min Sci* 36:191–215
- Brudy M, Zoback M, Fuchs K, Rummel F, Baumgärtner J (1997) Estimation of the complete stress tensor to 8-km depth in the KTB scientific drill holes: implications for crustal strength. *J Geophys Res* 102:18453–18475
- Chang C, Lee JB, Kang T-S (2010) Interaction between regional stress state and faults: complementary analysis of borehole in situ stress and earthquake focal mechanism in southeastern Korea. *Tectonophysics* 485:164–177
- Chang C, Jo Y, Quach N, Shinn YJ, Song I, Kwon YK (2016) Geomechanical characterization for the CO₂ injection test site, offshore Pohang Basin, SE Korea. In: 50th U.S. rock mechanics/geomechanics symposium, American Rock Mechanics Association, Houston, TX, USA, pp 1–6, ARMA16-541
- Choi S, Park C, Synn J, Shin H (2008) A decade's experiences on the hydrofracturing in situ stress measurement for tunnel construction in Korea. In: Proceedings of the Korean Society for Rock Mechanics (KSRM) 2008 fall conference KSRM, Seoul, Korea, pp 79–88
- Colmenares L, Zoback M (2002) A statistical evaluation of intact rock failure criteria constrained by polyaxial test data for five different rocks. *Int J Rock Mech Min Sci* 39(6):695–729
- Cornet F (2015) Elements of crustal geomechanics. Cambridge University Press, Cambridge
- Fairhurst C (2003) Stress estimation in rock: a brief history and review. *Int J Rock Mech Min Sci* 40:957–973

- Fouial K, Alheib M, Baroudi H, Trentaux C (1998) Improvement in the interpretation of stress measurements by use of the overcoring method: development of a new approach. *Eng Geol* 49(3):239–252
- Haimson B, Cornet F (2003) ISRM suggested methods for rock stress estimation—part 3: hydraulic fracturing (HF) and/or hydraulic testing of pre-existing fractures (HTPF). *Int J Rock Mech Min Sci* 40:1011–1020
- Haimson B, Lee MY, Song I (2003) Shallow hydraulic fracturing measurements in Korea support tectonic and seismic indicators of regional stress. *Int J Rock Mech Min Sci* 40(7):1243–1256
- Hart R (2003) Enhancing rock stress understanding through numerical analysis. *Int J Rock Mech Min Sci* 40(7):1089–1097
- Heidbach O, Rajabi M, Reiter K, Ziegler M, WSM Team (2016) World stress map database release 2016. doi:10.5880/WSM.2016.001
- Hubbert MK, Willis DG (1957) Mechanics of hydraulic fracturing I. *US Geol Surv* 210:153–168
- Hudson J, Cooling C (1988) In situ rock stresses and their measurement in the UK—part I. The current state of knowledge. *Int J Rock Mech Min Sci Geomech Abstr* 25(6):363–370
- Hudson JA, Cornet FH (2003) Special issue on rock stress estimation. *Int J Rock Mech Min Sci* 40(7):955
- Jaeger JC, Cook NG, Zimmerman R (2009) *Fundamentals of rock mechanics*. Wiley, New York
- Kim H, Min KB, Bae S, Stephansson O (2016) Integrated in situ stress estimation by hydraulic fracturing and borehole observation at EXP-1 hole in Pohang of Korea. In: ISRM international symposium on in-situ rock stress. International Society for Rock Mechanics, Tampere, Finland, pp 333–342, ISRM-ISRS-2016-029
- Klee G, Bunger A, Meyer G, Rummel F, Shen B (2011) In situ stresses in borehole Blanche-1/South Australia derived from breakouts, core discing and hydraulic fracturing to 2-km depth. *Rock Mech Rock Eng* 44:531–540
- Kyung JB (2003) Paleoseismology of the Yangsan fault, southeastern part of the Korean peninsula. *Ann Geophys* 46(5):983–996
- Lee M, Haimson B (1989) Statistical evaluation of hydraulic fracturing stress measurement parameters. *Int J Rock Mech Min Sci Geomech Abstr* 26(6):447–456
- Lee TJ, Song Y, Yoon WS, Kim K, Jeon J, Min K, Cho Y (2011) The first enhanced geothermal system project in Korea. In: Proceedings of the 9th Asian geothermal symposium, Asian geothermal symposium, Kahoshima, Japan, pp 129–132
- Plumb RA, Hickman SH (1985) Stress-induced borehole elongation: a comparison between the four-arm dipmeter and the borehole televiewer in the Auburn Geothermal Well. *J Geophys Res* 90:5513–5521
- Rutqvist J, Tsang C-F, Stephansson O (2000) Uncertainty in the maximum principal stress estimated from hydraulic fracturing measurements due to the presence of the induced fracture. *Int J Rock Mech Min Sci* 37:107–120
- Shen B (2014) Development and applications of rock fracture mechanics modelling with FRACOD: a general review. *Geosyst Eng* 17(4):235–252
- Shen B, Stephansson O, Rinne M (2014) *Modelling ROCK FRACTURING PROCESSES*. Springer, Dordrecht
- Stephansson O, Zang A (2012) ISRM suggested methods for rock stress estimation—part 5: establishing a model for the in situ stress at a given site. *Rock Mech Rock Eng* 45(6):955–969
- Synn J-H, Park C, Lee B-J (2013) Regional distribution pattern and geo-historical transition of in situ stress fields in the Korean peninsula. *Tunn Undergr Space* 23:457–469
- Tingay M, Reinecker J, Müller B (2008) Borehole breakout and drilling-induced fracture analysis from image logs. *World Stress Map Project*, pp 1–8
- Vernik L, Zoback MD (1992) Estimation of maximum horizontal principal stress magnitude from stress-induced well bore breakouts in the Cajon Pass Scientific Research borehole. *J Geophys Res* 97(B4):5109–5119
- Walker J, Martin C, Dzik E (1990) Confidence intervals for in situ stress measurements. *Int J Rock Mech Min Sci Geomech Abstr* 27(2):139–141
- Wileveau Y, Cornet F, Desroches J, Blumling P (2007) Complete in situ stress determination in an argillite sedimentary formation. *Phys Chem Earth* 32(8):866–878
- Wiprut D, Zoback M (2000) Constraining the stress tensor in the Visund field, Norwegian North Sea: application to wellbore stability and sand production. *Int J Rock Mech Min Sci* 37(1):317–336
- Yoon KS, Jeon JS, Hong HK, Kim HG, Hakan A, Park JH, Yoon WS (2015) Deep drilling experience for Pohang enhanced geothermal project in Korea. In: Proceedings world geothermal congress 2015. International Geothermal Association, Melbourne, Australia, pp 1–11
- Zang A, Stephansson O (2010) *Stress field of the Earth's crust*. Springer, Dordrecht
- Zhou S (1994) A program to model the initial shape and extent of borehole breakout. *Comput Geosci* 20(7):1143–1160
- Zoback M (2007) *Reservoir geomechanics*. Cambridge University Press, Cambridge
- Zoback M, Moos D, Mastin L, Anderson R (1985) Well bore breakouts and in situ stress. *J Geophys Res* 90(B7):5523–5530
- Zoback M, Apel R, Baumgärtner J, Brudy M, Emmermann R, Engeser B, Fuchs K, Kessels W, Rischmüller H, Rummel F (1993) Upper-crustal strength inferred from stress measurements to 6-km depth in the KTB borehole. *Nature* 365:633–635
- Zoback M, Barton C, Brudy M, Castillo D, Finkbeiner T, Grollimund B, Moos D, Peska P, Ward C, Wiprut D (2003) Determination of stress orientation and magnitude in deep wells. *Int J Rock Mech Min Sci* 40(7):1049–1076